

Modeling of the Separation of the Enantiomers of 1-Phenyl-1-propanol on Cellulose Tribenzoate

Alberto Cavazzini, Krzysztof Kaczmarski,[†] Paweł Szabelski, Dongmei Zhou, Xiaoda Liu, and Georges Guiochon*

Department of Chemistry, The University of Tennessee, Knoxville, Tennessee, 37996-1600, and Division of Chemical and Analytical Sciences, Oak Ridge National Laboratory, Oak Ridge, Tennessee 37831

The competitive adsorption isotherms of *rac*-1-phenyl-1-propanol on cellulose tribenzoate were measured by competitive frontal analysis. The experimental data were fitted to four different isotherm models: Langmuir, Bi-langmuir, Langmuir–Freundlich, and Tóth. The fittings of the experimental data to all four models were satisfactory. It was excellent in the case of the Langmuir–Freundlich and the Tóth models. Overloaded elution profiles calculated with the Tóth isotherm were in good agreement with the experimental profiles in all the different experimental conditions investigated. This work extends to the case of binary mixtures the equivalence between the general rate and the lumped pore diffusion models already demonstrated for pure compounds when the ratio between the Stanton and the Biot numbers exceeds 5. The adsorption energy distribution for the Tóth isotherm was also calculated.

Although the production/purification of enantiomers can be performed in different ways, preparative liquid chromatography is becoming the most popular. Destruction of the unwanted isomer in the racemic mixture by enzymatic reactions and crystallization from the racemic mixture remain important but are often combined with chromatography. Effective and economical stereoselective synthesis is difficult and takes long to develop. They require a chiral starting substrate leading to the production of the desired enantiomer, involve numerous steps, most giving low reaction yields, and rarely give the enantiomeric purity required. A compromise between cost and effectiveness often leads to the synthesis of an enriched mixture from which the desired enantiomer is extracted by preparative LC. The same situation also arises with crystallization.¹ This explains why large-scale preparative chromatography has become the most attractive and useful procedure to separate and purify enantiomeric mixtures.^{2,3}

Direct chiral separations, using chiral stationary phases (CSPs), have important advantages with respect to other available techniques of enantiomeric purification. The large-scale production of a mixture moderately enriched in the desired enantiomer is faster and less expensive than the production of a pure enantiomer by a highly stereoselective synthesis or by recrystallization techniques. A large number of CSPs are now available. In some cases, these CSPs are suitable only for a few specific separations;^{4–6} often they are designed for molecules presenting some specific chemical functionalities.^{2,7}

Cellulose-based CSPs are made by coating a cellulose polymer on a wide-pore silica support. Before being coated on silica particles, the cellulose polymer is derivatized by introduction of specific groups (e.g., acetate, benzoate, and carbamate).^{7,8} These functionalities have an important role in the enantioselectivity of the CSP. On any glucose unit of the cellulose, there are five stereogenic centers, causing the polymer to have a high density of stereogenic sites available for diastereomeric associations. Thus, cellulose-based CSPs have a high saturation capacity, making them optimal for preparative purposes.⁹ The major limit of this kind of CSP is the limited number of suitable solvents. Usually, only nonpolar mobile phases, composed of hexane, heptane and methanol, or 2-propanol (up to 10%), can be used.^{9,10}

Despite the large number of chiral separations described, the mechanisms of interaction that control chiral separations are not yet well understood.² Few detailed, reliable experimental data are available.¹¹ Most of them refer to analytical separations made under linear conditions.^{12–20} These do not even allow the estima-

* Corresponding author: (tel) + 1-865-9740-733; (fax) + 1-865-9742-667; (e-mail) guiochon@utk.edu.

[†] On leave from the Faculty of Chemistry, Rzeszów University of Technology, W. Pola 2 St., 35-959, Rzeszów, Poland.

(1) Lorenz, H.; Sheehan, P.; Seidel-Morgenstern, A. *J. Chromatogr., A* **2001**, *908*, 201–214.

(2) Ahuja, S. *Chiral separations by chromatography*; Oxford University Press: Washington, DC, 2000.

(3) Ariens, E. *J. Med. Res. Rev.* **1986**, *6*, 451–466.

(4) Sellergren, B. *Chirality* **1989**, *1*, 63–68.

(5) Sajonz, P.; Kele, M.; Zhong, G.; Sellergren, B.; Guiochon, G. *J. Chromatogr., A* **1998**, *810*, 1–17.

(6) Chen, Y.; Kele, M.; Sajonz, P.; Sellergren, B.; Guiochon, G. *Anal. Chem.* **1999**, *71*, 928–938.

(7) Beesley, T. E.; Scott, R. P. W. *Chiral chromatography*; John Wiley & Sons: Chichester, U.K., 1998.

(8) Shibata, T.; Okamoto, I.; Ishii K. *J. Liq. Chromatogr.* **1986**, *9*, 313–340.

(9) Francotte, E.; Junker-Buchheit, A. *J. Chromatogr.* **1992**, *576*, 1–45.

(10) Charton, F.; Jacobson, S. C.; Guiochon, G. *J. Chromatogr., A* **1993**, *630*, 21–35.

(11) Jacobson, S. C.; Golshan Shirazi, S.; Guiochon, G. *J. Chromatogr., A* **1990**, *522*, 23–36.

(12) Armstrong, D. W.; Han, S. M. *Crit. Rev. Anal. Chem.* **1988**, *19*, 175–224.

(13) Pirkle, W. H.; Pochapsky, T. C. *Chem. Rev.* **1989**, *89*, 347–362.

(14) Allenmark, S.; Bomgren, B.; Boren, H. *J. Chromatogr., A* **1982**, *237*, 473–477.

(15) Allenmark, S.; Bomgren, B.; Boren, H. *J. Chromatogr., A* **1983**, *264*, 63–68.

tion of reliable thermodynamic parameters at infinite dilution because the separation of the enantioselective contribution to retention from that of nonselective interactions is impossible with such data. Furthermore, chiral recognition is complex. The reversible diastereomeric equilibrium between the solute enantiomers and the CSP^{2,7} is usually reached by the combined effect of different molecular interactions, including hydrogen bonding, electrostatic and dipole–dipole interactions, charge-transfer interactions, and hydrophobic interactions. Finally, the steric fit represents another important, sometimes the dominant mechanism of chiral separation.^{4–6}

Different models were proposed to describe chiral separation mechanisms. The Dalglish model²¹ is based on a three-point interaction between the enantiomer and the CSP. This concept is often used for the description of the separation mechanism of small chiral molecules.²² Although this model has long been accepted as the only one able to explain enantiomeric separations, there is now ample experimental evidence that chiral recognition does not always require a three-point interaction, particularly with CSPs such as cellulose derivatives that have a high density of stereogenic centers².

Wainer et al.²⁰ showed that a proper steric fit seems to play a fundamental role in chiral separations. The cellulose surface presents grooves in which one enantiomer can fit better than the other, giving a stronger adsorption. The mechanism proposed by Wainer et al. involves several steps: (a) the formation of diastereomeric solute–CSP complexes, through hydrogen bonding; (b) the stabilization of this complex through insertion of the aromatic portion of the solute into a cavity of the CSP; and (c) a chiral discrimination between enantiomeric solutes due to the difference in their steric fit in the chiral cavity. However, in the separation of a molecule like 1-phenyl-1-propanol (PP), it is practically impossible to differentiate between the first step (hydrogen bond formation) and the second step (stabilization process). The proximity between hydroxyl and aromatic moieties suggests that these two processes are almost simultaneous. Furthermore, besides the CSP structure, other variables must be accounted for. The nature of the alcohol used as the mobile-phase additive is important. By contrast with other cases in HPLC, the mobile-phase modifier seems to affect the separation more through a steric hindrance effect in the grooves of the CSP than through competitive adsorption. The same amount of two different modifiers (e.g., two different alkanols) bound in similar density near the inclusion site modifies the steric environment in different ways that may cause dramatic changes in both the retention factors and the selectivity.^{2,19,20}

The behavior of band profiles at high concentrations (or large feed samples) is well known. These bands become strongly

unsymmetrical and broaden and their resolution degrades.²³ This phenomenon is due to the nonlinear behavior of the adsorption isotherms of the feed components and to the competition between these different compounds for adsorption on the stationary phase. The separation of large-size samples is difficult and its assessment without the help of a model nearly impossible.²³ The optimization of a separation needs proper models of its thermodynamics and kinetics that are able to predict the degree of band overlapping. When such models are available, the optimal conditions for maximum production rate or minimum production cost at a defined product purity can be derived. The purpose of this work is to illustrate how an accurate modeling of chiral preparative chromatography is possible.

Numerous mathematical models are available to account for the band profiles obtained in chromatography and in other adsorption-based separation processes under different experimental conditions.^{23–25} The equilibrium-dispersive (ED) model is most often used when the mass resistances are small.²³ More sophisticated models include the general rate (GR) model that accounts for all the kinetic phenomena affecting the separation, the lumped pore diffusion (POR) model, and the transport-dispersive (TD) model.^{26–30} Recently Kaczmarski et al. compared these models and showed the narrow limits of the TD model.³¹ These authors demonstrated also that the rate coefficients derived from a fitting of experimental data to this model do not have the clear physical meaning usually attributed to them. For these reasons, we used only the POR and the GR models in this work to account for the experimental data.

THEORETICAL SECTION

1. GR Model. When the GR model is used to describe the chromatographic process, all the physicochemical phenomena involved in the thermodynamics and kinetics of adsorption are accounted for. These include the adsorption–desorption mechanism at the actual sites, axial dispersion, and all the mass-transfer resistances, namely, (a) the external mass transfer of the solute molecules from the bulk phase to the external surface of the adsorbent particles and (b) the diffusive transport through the pores of these particles toward the pore surface and back. The modeling of all the contributions to these resistances involves a large number of parameters that must be evaluated. Some of them should be determined independently for a predictive use of the model, but their accurate determination is often difficult (e.g., the external bed porosity and the adsorbent particle porosity).

- (16) Allenmark, S.; Bomgren, B.; Boren, H. *J. Chromatogr., A* **1984**, *316*, 617–624.
- (17) Allenmark, S.; Andersson, S.; Bojarski, J. *J. Chromatogr., A* **1988**, *436*, 479–483.
- (18) Allenmark, S. *Chem. Scr.* **1982**, *20*, 5–10.
- (19) Wainer, I. W.; Alembik, M. C. *J. Chromatogr.* **1986**, *358*, 85–93.
- (20) Wainer, I. W.; Stiffin, R. M.; Shibata, T. *J. Chromatogr.* **1987**, *411*, 137–151.
- (21) Dalglish, C. E. *Biochem. J.* **1952**, *52*, 3–14.
- (22) Pirkle, W. H. In *Chromatography and Separation Chemistry*; Ahuja, S., Ed.; ACS Symposium Series 297; American Chemical Society: Washington, DC, 1986.

- (23) Guiochon, G.; Shirazi, S. G.; Katti, A. M. *Fundamentals of preparative and nonlinear chromatography*; Academic Press: Boston, MA, 1994.
- (24) Ruthven, D. M. *Principles of adsorption and adsorption processes*; Wiley: New York, 1984.
- (25) Suzuki, M. *Adsorption Engineering*; Elsevier: Amsterdam, The Netherlands, 1990.
- (26) Kaczmarski, K.; Storti, G.; Mazzotti, M.; Morbidelli, M. *Comput. Chem. Eng.* **1997**, *21*, 641–660.
- (27) Berninger, J. A.; Whitley, R. D.; Zhang, X.; Wang, N. H. L. *Comput. Chem. Eng.* **1991**, *15*, 749–768.
- (28) Sajonz, P.; Guan-Sajonz, H.; Zhong, G. M.; Guiochon, G. *Biotechnol. Progr.* **1997**, *12*, 170–178.
- (29) Miyabe, K.; Guiochon, G. *Biotechnol. Progr.* **1999**, *15*, 740–752.
- (30) Miyabe, K.; Guiochon, G. *J. Chromatogr., A* **2000**, *866*, 147–171.
- (31) Kaczmarski, K.; Antos, D.; Guan – Sajonz, H.; Guiochon, G. *J. Chromatogr., A* **2001**, *925*, 1–17.

When the mass-transfer resistance in the bulk phase is much smaller than the mass-transfer resistance inside the pores and axial dispersion has a negligible influence on band broadening, the number of parameters needed in the model is reduced. Such conditions were fulfilled, e.g., for bovine serum albumin (a large protein molecule) on an anion-exchange resin.³¹ We will apply now this model to the chiral separation of a relatively small molecule, 1-phenyl-1-propanol.

The complete discussion of the GR model can be found in many places.^{23–25} We present here only a brief description of its fundamental equations. They include two mass balance equations for each feed component. The former is the mass balance in the mobile phase percolating through the bed of packing material, and the latter, the mass balance inside the packing particles, involving both the stagnant mobile phase and the adsorbed monolayer. These equations are completed by suitable initial and boundary conditions and by the isotherm equation.^{27,32–34}

1.1. Mass Balance Equations. (1) *Mass Balance of the i th Component in the Mobile Fluid Phase.* This balance is classically written as

$$\epsilon_e \frac{\partial C_i}{\partial t} + u \frac{\partial C_i}{\partial z} = \epsilon_e D_L \frac{\partial^2 C_i}{\partial z^2} - (1 - \epsilon_e) k_{\text{ext},i} a_p [C_i - C_{p,i}(r = R_p)] \quad (1)$$

where ϵ_e is the external porosity, C_i and $C_{p,i}$ are the concentrations of component i th in the mobile phase and inside the particle pores, respectively, t is the time, z is the distance along the column, u is the superficial linear mobile-phase velocity, D_L is the axial dispersion coefficient, $k_{\text{ext},i}$ is the external mass-transfer resistance for component i , R_p is the equivalent particle radius, r is the radial coordinate, and $a_p (= 3/R_p)$ is the external surface area per unit volume of the adsorbent particles (assumed to be all spherical and to have all the same radius).

(2) *Mass Balance of the i th Component Inside the Solid-Phase Particles.*

$$\epsilon_p \frac{\partial C_{p,i}}{\partial t} + (1 - \epsilon_p) \frac{\partial q_i}{\partial t} = D_{\text{eff}} \frac{1}{r^2} \frac{\partial}{\partial r} \left(r^2 \frac{\partial C_{p,i}}{\partial r} \right) \quad (2)$$

where ϵ_p is the internal (particle) porosity, q_i is the stationary-phase concentration, and D_{eff} the effective (or inside-pore) diffusion coefficient.

1.2. Initial Conditions. We have two partial differential equations and need one initial condition for each

$$C_i(0, \mathbf{z}) = 0 \quad (3)$$

$$C_{p,i}(0, r, \mathbf{z}) = 0; \quad q_i(0, r, \mathbf{z}) = 0; \quad \text{for } 0 < \mathbf{z} < L; \\ 0 < r < R_p \quad (4)$$

where the subscript 0 indicates initial values and L is the column length.

1.3. Boundary Conditions. For eq 1, we have two boundary conditions. The former at the column inlet, the latter at the column exit. The condition for $t > 0$ and $\mathbf{z} = 0$ is

$$u_t C_{t,i} - u(0) C(0) = -\epsilon_e D_L (\partial C_i / \partial z) \quad (5)$$

$$C_{t,i} = C_{t,i} \quad \text{for } 0 < t < t_p$$

$$C_{t,i} = 0 \quad \text{for } t_p < t$$

where t_p is the injection time. The condition for $t > 0$ and $\mathbf{z} = L$ is

$$\partial C_i / \partial z = 0 \quad (6)$$

For eq 2, there are again two boundary conditions, for $t > 0$ and $r = R_p$

$$D_{\text{eff}} \frac{\partial C_{p,i}(t, r)}{\partial r} = k_{\text{ext},i} [C_i - C_{p,i}(t, r)] \quad (7)$$

and for $t > 0$ and $r = 0$

$$\partial C_{p,i}(t, r) / \partial r = 0 \quad (8)$$

Combined with the phase equilibrium isotherm, eqs 1–8 constitute the mathematical translation of the GR model.

2. Lumped Pore Diffusion Model. When the effective diffusion coefficient in an adsorbent material is not too low, the POR model can be used instead of the more complex GR model for calculating band profiles.^{35,36} Kaczmarski and Antos³² found that the POR model is numerically equivalent to the GR model when

$$Pe > 100, \quad St/Bi > 5 \quad (9)$$

where Pe is the Peclet number defined by $Pe = uL/D_L\epsilon_e$, St is the Stanton number, $St = K_{\text{ext}} a_p L \epsilon_e / u$, and Bi is the Biot number, $Bi = K_{\text{ext}} d_p L \epsilon_e / 2D_{\text{eff}}$. In these equations, d_p is the average particle diameter and the other symbols are defined as before.

In the POR model, the mass balances of the i th component in the mobile and the solid phases are simplified and written as follows:

$$\epsilon_e \frac{\partial C_i}{\partial t} + u \frac{\partial C_i}{\partial z} = \epsilon_e D_L \frac{\partial^2 C_i}{\partial z^2} - (1 - \epsilon_e) k_i a_p (C_i - \bar{C}_{p,i}) \quad (10)$$

$$\epsilon_p \frac{\partial \bar{C}_{p,i}}{\partial t} + (1 - \epsilon_p) \frac{\partial \bar{q}_i}{\partial t} = k_i a_p (C_i - \bar{C}_{p,i}) \quad (11)$$

where $\bar{C}_{p,i}$ and \bar{q}_i denote average concentrations and k_i , the

(32) Kaczmarski, K.; Antos, D. *J. Chromatogr., A* **1996**, 756, 73–87.

(33) Gu, T.; Tsai, G. J.; Tsao, G. T. In *Advances in Biochemical Engineering Biotechnology*; Fiechter, A., Ed.; Springer-Verlag: New York, 1993.

(34) Kaczmarski, K. *Comput. Chem. Eng.* **1996**, 20, 49–64.

(35) Morbidelli, M.; Servida, A.; Storti, G.; Carra, S. *Ind. Eng. Chem. Fund.* **1982**, 21, 123–131.

(36) Morbidelli, M.; Storti, G.; Carra, S.; Niederjaufer, G.; Pontoglio, A. *Chem. Eng. Sci.* **1984**, 39, 383–393.

overall mass-transfer coefficient for component i , is given by

$$k_i = \left[\frac{1}{k_{\text{ext},i}} + \frac{1}{k_{\text{int},i}} \right]^{-1} \quad (12)$$

where k_{int} is the internal mass-transfer coefficients. k_{int} is calculated by the following equations:

$$k_{\text{int}} = 10D_{\text{eff}}/d_p \quad (13)$$

and

$$D_{\text{eff}} = \epsilon_p D_m / \gamma \quad (14)$$

where D_m is the molecular diffusivity (see later) and γ is the internal tortuosity factor calculated by²³

$$\gamma = (2 - \epsilon_p)^2 / \epsilon_p \quad (15)$$

The initial and the boundary conditions for the POR model are similar to those used in the GR model.

3. Dispersion Coefficient and External Mass-Transfer Coefficient. The knowledge of the external mass transfer, k_{ext} , the molecular diffusivity, D_m , and the dispersion coefficient, D_L , is necessary to use the GR or the POR models. In this work, we used three empirical or semiempirical correlations to evaluate these parameters.

The Wilson–Geankoplis equation:³⁷

$$Sh = (1.09/\epsilon_e) Sc^{1/3} Re^{1/3} \quad (16)$$

expresses the Sherwood number, Sh , as a function of the external porosity, and of the Schmidt and Reynolds numbers, respectively, Sc and Re . These numbers are defined by³⁸

$$Sc = \eta / \rho D_m < \quad (17)$$

and

$$Re = \rho u d_p / \eta \quad (18)$$

where η is the viscosity and ρ the fluid density. Because the Sherwood number is defined as³⁸

$$Sh = k_{\text{ext}} d_p / D_m \quad (19)$$

we can use eq 16 together with eq 19 to calculate k_{ext} when D_m is known.

For the calculation of the molecular diffusion coefficient in the bulk phase, the Wilke–Chang correlation can be used.^{23,38} This

equation gives an excellent approximation for molecules having a moderate molecular weight. Its formulation is

$$D_m = 7.4 \times 10^{-8} \frac{(\alpha_A M_s)^{0.5} T}{\eta V_m^{0.6}} \quad (20)$$

where T is the absolute temperature, V_m is the molar volume of the liquid solute at its normal boiling point, M_s is the molecular weight of the solvent, and α_A is a constant that accounts for solute–solvent interactions.

Finally, the dispersion coefficient was calculated from Gunn equation³⁹

$$\epsilon_e \frac{D_L}{d_p u} \left\{ \frac{Re Sc}{4\alpha_1^2 (1 - \epsilon_e)} (1 - p)^2 + \frac{(Re Sc)^2}{16\alpha_1^4 (1 - \epsilon_e)^2} p(1 - p)^3 \right. \\ \left. \left[\exp\left(\frac{-4\alpha_1^2 (1 - \epsilon_e)}{p(1 - p) Re Sc}\right) - 1 \right] \right\} (1 + \sigma_v^2)^2 + \frac{\sigma_v^2}{2} + \frac{\epsilon_e}{\tau Re Sc} \quad (21)$$

where α_1 is the first root of the zero-order Bessel function, τ is the bed package tortuosity factor (assumed equal to 1.4 according to ref 39), and σ_v^2 is the dimensionless variance of the distribution of the ratio between fluid linear velocities and average velocity over the column cross section, assumed in this work equal to zero. p is a parameter defined by³⁹

$$p = 0.17 + 0.33 \exp(-24/Re) \quad (22)$$

4. POR and GR Models Numerical Solution. Both the POR and the GR models were solved using programs based on implementations of the method of orthogonal collocation on finite element.^{23,26,27} The set of discretized ordinal differential equations was solved with the Adams–Moulton method, implemented in the VODE procedure.⁴⁰ The relative and absolute errors of the numerical calculations were equal to 1×10^{-6} and 1×10^{-8} , respectively.

EXPERIMENTAL SECTION

1. Equipment. A HP 1090 liquid chromatography (Hewlett-Packard, Palo Alto, CA) was used for all the experimental determinations. This instrument was equipped with a multi-solvent delivery system, an automatic sample injector with a 25- μ L loop, a diode array detector, and a computer data station. A back pressure regulator (100 psi, Upchurch, Scientific Oak Arbor, WA) was inserted downstream of the detector unit to control the pressure inside the detector and the average column pressure.

2. Materials. (1) *Mobile Phase and Chemicals.* The mobile phase was a solution of *n*-hexane and 2-propanol (97:3, v/v). Hexane and 2-propanol were HPLC grade solvents from Fisher Scientific, Fair Lawn, NJ. 1,3,5-Tri-*tert*-butylbenzene was purchased from Aldrich (Milwaukee, WI). The racemic mixture of 1-Phenyl-

(37) Wilson, E. J.; Geankoplis, C. J. *Ind. Eng. Chem. Fundam.* **1966**, *5*, 9–14.

(38) Reid, R. C.; Prausnitz, J. M.; Sherwood, T. K. *The properties of gases and liquids*; McGraw-Hill: New York, 1997.

(39) Gunn, D. J. *Chem. Eng. Sci.* **1987**, *42*, 363–373

(40) Brown, P. N.; Hindmarsh, A. C.; Byrne, G. D. *Variable Coefficient Ordinary Differential Equation Solver*; procedure available on <http://www.netlib.org>.

1-PrOpanol, also from Aldrich, was previously purified in our laboratory.⁴¹

(2) *Column.* A 20 × 1.0 cm stainless steel column, packed in-house⁴¹ with Chiralcel OB (cellulose tribenzoate coated on a silica support; Daicel, Tokyo, Japan) was used for all determinations and experiments. The average particle diameter of the packing material was 20 μm. The total column porosity, measured by injecting 1,3,5-tri-*tert*-butylbenzene, a compound that was considered as unretained on this surface,^{10,41} was 0.715. The holdup time was 5.59 min. The efficiency of the column measured with the same compound was ~1000 theoretical plates.

3. Procedures for Isotherm Determination. (1) *Measurements of Experimental Data.* All the experimental data were measured at room temperature (22.5–24.5 °C), with a 2.0 mL/min mobile-phase flow rate. The retention factors for the less and the more retained enantiomers were respectively 1.66 and 2.17; the selectivity factor was 1.31. Although the single enantiomers ((*S*)-PP and (*R*)-PP) were not available, we assumed the more retained compound to be (*R*)-PP and the less retained (*S*)-PP, according to ref 41. Efficiency as well as selectivity determinations were performed several times during the experimental work. Their reproducibilities are characterized by a RSD of 1%. The wavelength (λ) used under linear conditions was 254 nm.

The competitive isotherm data were measured by frontal analysis (FA), the UV detector signal being monitored at λ = 280 nm. The same 8 value was used for the acquisition of overloaded profiles. The detector was calibrated several times during the experimental work and every time an overloaded profile was recorded. The calibration curve was nonlinear, even at relatively low concentrations. It was approximated by the cubic spline method. The reproducibility between different calibration curves was no better than 3–5%.

FA was performed in the conventional way, using the available multichannel solvent delivery system.²³ One channel was used to deliver the sample solution and the other to pump the pure mobile phase. Both solvent streams are mixed in the mixing chamber. The minimum sample volume necessary to reach the plateau concentration was 20 mL. The column was reequilibrated with pure mobile phase after each injection. The total range of concentration investigated was between 0.01 and 6 g/L (given as the racemic mixture concentration or total enantiomer concentration). Thirteen data points were acquired in the concentration range between 0.01 and 1.0 g/L and 9 points in the range between 1.0 and 6.0 g/L. All the measurements were repeated three times. The isotherm data were calculated by averaging the corresponding concentration data.

(2) *Modeling of the Experimental Data.* In all cases, the best numerical values of the isotherm parameters were estimated by fitting the experimental adsorption data to the model selected, using the least-squares Marquardt method modified by Fletcher.⁴² These parameters are listed in Table 1. The goodness of fit in the different cases can be estimated by the values of the Fisher parameters calculated according to refs 43 and 44 and reported

Table 1. Best Estimates of the Parameters for the Different Isotherm Models and Fisher Parameter^{43,44} Values

isotherm type	parameters	Fisher test
Langmuir	$q_s = 47 \pm 1.0$ $K_1 = 0.0865 \pm 0.003$ $K_2 = 0.110 \pm 0.003$	9190
biLangmuir	site 1, nonselective $q_{s,1} = 41 \pm 1.5$ $K_{1,1} = 0.098 \pm 0.005$ $K_{2,1} = 0.098 \pm 0.005$ site 2, selective $q_{s,2} = 5.6 \pm 1.0$ $K_{1,2} = 0$ $K_{2,2} = 0.196 \pm 0.05$	8970
Langmuir–Freundlich	$q_s = 54.9 \pm 3.0$ $K_1 = 0.0716 \pm 0.005$ $K_2 = 0.091 \pm 0.006$ $\nu_1 = 0.96 \pm 0.01$ $\nu_2 = 0.96 \pm 0.01$	19650
Tóth	$q_s = 70 \pm 11$ $K_1 = 0.061 \pm 0.008$ $K_2 = 0.078 \pm 0.001$ $\nu = 0.77 \pm 0.06$	19590

in the same table. On the basis of this Fisher test, the model that better correlates the data is the one that exhibits the highest value of this parameter.

RESULTS AND DISCUSSION

1. Equilibrium Isotherms. The adsorption data for the PP enantiomers on tribenzoate cellulose CSP were modeled using four competitive adsorption-isotherm models: the Langmuir, the biLangmuir (BL), the Langmuir–Freundlich (LF), and the Tóth (T) models.^{23,45}

(1) *Langmuir Isotherm.* This isotherm model is the one most frequently used to account for competitive and noncompetitive adsorption data in chromatography. The equations for the competitive Langmuir model for two components are written

$$q_i = \frac{q_s K_i C_i}{1 + K_1 C_1 + K_2 C_2}, \quad i = 1, 2 \quad (23)$$

where q_s is the saturation capacity, equal for both components, and K_i denotes the equilibrium (Langmuir) constant for the i th component.

An adsorption isotherm represents all the possible interactions, attractive as well as repulsive, between the solute molecules and the stationary phase. With enantiomeric mixtures, the diastereomeric or enantioselective interactions are the only ones responsible for the separation. If a pure Langmuir competitive isotherm is considered, it is implicitly assumed that (a) the nonselective interactions have a negligible contribution to the retention of the enantiomers and (b) the energies of all the possible enantioselective interactions are close enough that they can be averaged, so a single adsorption energy and a single adsorption constant

(41) Khattabi, S.; Cherrack, D. E.; Fisher, J.; Jandera, P.; Guiochon G. J. *Chromatogr., A* **2000**, *877*, 95–107.

(42) Fletcher, R. *A Modified Marquardt sub-routine for nonlinear least squares*; AERE-R6799-Harwell.

(43) Ajnazarova, S. L.; Kafarov, V. V. *Methods for experimental optimization in chemical technology*; Vishaia Shkola: Moscow, 1985.

(44) Quiñones, I.; Ford, J. C.; Guiochon, G. *Chem. Eng. Sci.* **2000**, *55*, 909–929.

(45) Jaroniec, M.; Madey, R. *Physical Adsorption on Heterogeneous Solids*; Elsevier: Amsterdam, 1988.

can be defined, which characterize all the adsorption sites on the surface. Obviously, these average energies and constants are different for the two enantiomers. However, with this isotherm, more sophisticated models for enantiomeric separation cannot be proposed. Table 1 reports the best values of the isotherm parameters (second line in Table 1). Khattabi et al.⁴¹ had also used this model to fit the (*R*)-PP and (*S*)-PP experimental data that they obtained on Chiralcel OB with a mobile phase composed of *n*-hexane and ethyl acetate (95:5, v/v). Although the fitting of our experimental data to the Langmuir isotherm is also fairly good in this case, leading to a relatively high value of the Fisher test, we observed, as these authors did, some serious inconsistencies between experimental band profiles at high concentrations and profiles calculated with this Langmuir isotherm (see later).

(2) *BiLangmuir Isotherm*. This model is directly derived from the Langmuir isotherm. It assumes that the adsorbent surface consists of two different types of independent adsorption sites. Under this assumption, the adsorption energy distribution can be modeled by a bimodal discrete probability density function, where two spikes (δ -Dirac functions) are located at the average adsorption energy of the two kinds of sites.⁴⁶ The BL model can be extended to account for competitive adsorption in the same way and with the same conditions of validity as for the Langmuir competitive isotherm.²³ For thermodynamic consistency, each one of the two saturation capacities should be the same for the two enantiomers. Although the BL isotherm is an ideal model (like the Langmuir isotherm), it is often successful in describing the adsorption of enantiomers on CSPs.⁴⁷ The reason is that, because of their specific physicochemical characteristics, enantiomeric systems fit most of the theoretical assumptions under which the BL model holds.^{23,48} Note, however, that this comment does not apply to CSPs based on certain chiral polymers such as cellulose or amylose derivatives.⁴⁷

When the BL isotherm is used to model the adsorption data of enantiomers, it is assumed that one type of site consists of the enantioselective sites (the stronger type) while the second type, the weaker one, accounts for all the other possible, nonselective interactions.^{10,23,47} The equation of the BL isotherm is

$$q_i = \frac{q_{s,1}K_{i,1}C_i}{1 + K_{1,1}C_1 + K_{2,1}C_2} + \frac{q_{s,2}K_{i,2}C_i}{1 + K_{1,2}C_1 + K_{2,2}C_2}, \quad i = 1, 2 \quad (24)$$

where $q_{s,1}$ and $q_{s,2}$ are the saturation capacities for the first and the second type of sites, respectively, and $K_{i,j}$ is the equilibrium constant of i th component on the j th type of sites ($j = 1, 2$). For the formulation in eq 24 to be consistent with the assumption that the first type of site accounts for the nonselective interactions, the coefficients $K_{1,1}$ and $K_{2,1}$ must be the same for both enantiomers.

The best values of the parameters of the BL isotherm for our data are reported in the third row of Table 1. It is noteworthy that the enantioselective sites (type 2) are seen only by the more

retained enantiomer. This is expressed by the fact that, although the data were fitted to eq 24, the equilibrium constant of the less retained compound ($i = 1$, (*S*)-PP) on the selective sites ($K_{1,2} = 0$) is equal to zero. By contrast, the weaker nonselective sites are recognized by both enantiomers. The value of the ratio $q_{s,2}/q_{s,1}$ suggests that only ~12% of the surface is covered with enantioselective sites. This value accords with some properties of cellulose-based CSP already described.²

As mentioned earlier, the BL isotherm model assumes that the surface of the adsorbent considered consists of patches of two types of independent and homogeneous sites. However, although acceptable for proteins that have exceptionally well-defined enantioselective adsorption sites, this assumption of energetic homogeneity is an idealization that is questionable in the case of cellulose-based CSPs.^{23,47} Due to the imperfections of the chiral surface and to the large number of possible sorbate/sorbent interactions during the chiral recognition process, a more realistic isotherm should account for a continuous distribution of adsorption energies.⁴⁵

(3) *Langmuir–Freundlich Isotherm*. This model is often successfully used to describe adsorption on heterogeneous surfaces. Like the competitive Langmuir isotherm, the competitive LF model requires equality of the saturation capacity (for both components) to be thermodynamically consistent.²³ Besides, it has the serious inconvenience of predicting that the retention time becomes infinite under analytical conditions (i.e., at infinite dilution). In the case of two components, the following equation describes the competitive LF isotherm:

$$q_i = \frac{q_s K_i C_i^{\nu_i}}{1 + K_1 C_1^{\nu_1} + K_2 C_2^{\nu_2}}, \quad i = 1, 2 \quad (25)$$

The coefficients ν_1 and ν_2 , smaller than unity, are the heterogeneity parameters. They characterize the degree of heterogeneity of the surface. If the heterogeneity parameters are equal to 1, the competitive LF model reduces to the Langmuir model. The best estimates of the values of the LF parameters are listed in the fourth row of Table 1. Very similar values are obtained for the two heterogeneity parameters and they are close to unity. The Fisher parameter is larger than for the two models studied previously, indicating an improved quality of the fit of the experimental data to the isotherm model.

(4) *Tóth Isotherm*. Finally, the adsorption data were fitted to the Tóth isotherm model. The quality of the fit of the experimental data to the isotherm model is the same as in the LF case (see Fisher test values, Table 1, last row). The Tóth isotherm was originally derived for the study of gas–solid equilibria. However, like the Langmuir isotherm model, it can be extended to the description of liquid–solid system. This isotherm has some characteristics similar to those of the LF isotherm. Both assume a continuous and possibly wide adsorption energy distribution. Unlike the LF isotherm, however, the Tóth isotherm has a finite Henry constant, hence predicts finite retention times at infinite dilution. Since the analytical chromatograms obtained for 1-phenyl-1-propanol do not exhibit significant tailing, we preferred the Tóth model to account for our data and to calculate overloaded band profiles.

(46) Cavazzini, A.; Remelli, M.; Dondi, F.; Felinger, A. *Anal. Chem.* **1999**, *71*, 3453–3462.

(47) Götmar, G.; Fornstedt, T.; Guiochon, G. *Chirality* **2000**, *12*, 558–564.

(48) Jacobson, S.; Golshan-Shirazi, S.; Guiochon, G. *J. Am. Chem. Soc.* **1990**, *112*, 6492–6498.

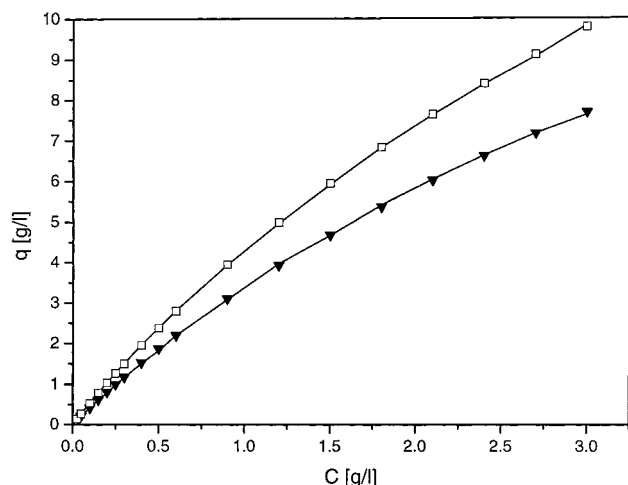


Figure 1. Experimental competitive adsorption data (symbols) and best Tóth isotherms (solid lines). Symbols: \square , (R)-PP; \blacktriangledown , (S)-PP.

The equation of the competitive Tóth isotherm is⁴⁵

$$q_i = \frac{q_s K_i C_i}{[1 + (K_1 C_1 + K_2 C_2)^\nu]^{1/\nu}}, \quad i = 1, 2 \quad (26)$$

where ν is the common heterogeneity parameter. Unlike the LF isotherm, the heterogeneity parameter of the Tóth model is the same for both components, an assumption that, in the present case, is consistent with the observation (Table 1, fourth and fifth rows) that the two heterogeneity coefficients of the LF models are practically equal. Thus, the Tóth model uses only four parameters, one parameter more than the Langmuir model and one less than the BL model. This is another of its practical advantages, even though physical meaning may be sacrificed to fitting quality. For the sake of thermodynamic consistency, the same saturation capacity was assumed for the two enantiomers.²³

Figure 1 compares the experimental adsorption competitive data (symbols) and the best isotherms (continuous lines) obtained with the Tóth model. The agreement is excellent. A "reasonable" physical model would assume a biTóth isotherm, with one Tóth component for each of the two types of sites, enantioselective and nonselective. Unfortunately, such a model would have eight coefficients. In view of the agreement observed between the experimental and calculated isotherms (Figure 1), there is no justification for this overmassage of the data. There was no point either in acquiring the data in a much wider concentration range.⁴⁷ The behavior of this CSP is very different from that of immobilized proteins.

2. Energy Distribution. In gas–solid equilibrium studies, the adsorption energy distribution is derived from the adsorption isotherm data by solving the following integral equation:

$$q(P) = \int_{\Phi_E} q(P, E) f(E) dE \quad (27)$$

where E is the adsorption energy, $f(E)$ is its probability density distribution function, and $\theta(P, E)$ is the so-called local isotherm

which defines the microscopic model of adsorption.^{45–49} P is the equilibrium partial pressure. Φ_E represents the physical domain of adsorption energies. Because the gas–solid equilibrium constant, K , is related to the adsorption enthalpy, E_a , via

$$K = K_0 \exp(E_a/RT) \quad (28)$$

where R is the ideal gas constant and K_0 , in the simplest adsorption model is a function only of the temperature,⁵⁰ eq 27 can be rewritten in terms of the equilibrium constant as

$$q(P) = \int_{\Phi_K} \theta(P, K) F(K) d \ln K \quad (29)$$

where the integral must be calculated in the equilibrium constant range, Φ_K . $F(K)$ is the probability density function for the equilibrium constant distribution. From a physical point of view, $F(K) d \ln K$ indicates the fraction of sites with an equilibrium constant between $\ln K$ and $\ln K + d \ln K$.

The application of these results to liquid–solid adsorption is far from straightforward. First, the assumption of a constant value for the preexponential factor K_0 (at constant temperature) represents a reasonable approximation only for the adsorption of gas mixtures on a heterogeneous surface. In the case of competitive liquid–solid equilibria, this assumption is not acceptable. On the contrary, in most cases, the entropic contribution to adsorption is determinant for the separation. In such cases, the well-known relationship between equilibrium constants and changes in the free Gibbs adsorption energy, ΔG , can be used:

$$K = \exp(-\Delta G/RT) \quad (30)$$

Using eq 30 and substituting concentration (C) for solute partial pressure (P), eq 29 can be rewritten as

$$q(C)/q_s = \int_{\Phi} X(C, K) \Phi(K) d \ln K \quad (31)$$

where $X(C, K)$ expresses the local isotherm model (now, a function of concentration) and $\Phi(K)$ is the equilibrium constant probability density function.

The solution of eq 27 or eq 31 with no further assumption regarding the overall isotherm or the local isotherm can be obtained by numerical methods or analytical approximations.^{45,49,51–54} It can be shown that the problem is ill posed from a mathematical point of view and most numerical algorithms do not give reliable results. In some cases, however, an analytical solution for eqs 27 and 31 does exist. Well-specified hypotheses regarding both the local and the overall adsorption isotherms must be made and they are unrealistic in most cases.

(49) Rudziński, W.; Everett, D. H. *Adsorption of gases on heterogeneous surfaces*; Academic Press: New York, 1992.

(50) De Boer, J. H. *The dynamical character of adsorption*; Clarendon Press: Oxford, U.K., 1968.

(51) Re, N. J. *Colloid Interface Sci.* **1994**, *166*, 191–207.

(52) Mechanick, J. I.; Peskin, C. S. *Anal. Biochem.* **1986**, *157*, 221–235.

(53) Stanley, B. J.; Guiochon, G. J. *Phys. Chem.* **1993**, *97*, 8098–8104.

(54) Stanley, B. J.; Guiochon, G., *Langmuir* **1994**, *10*, 4278–4285.

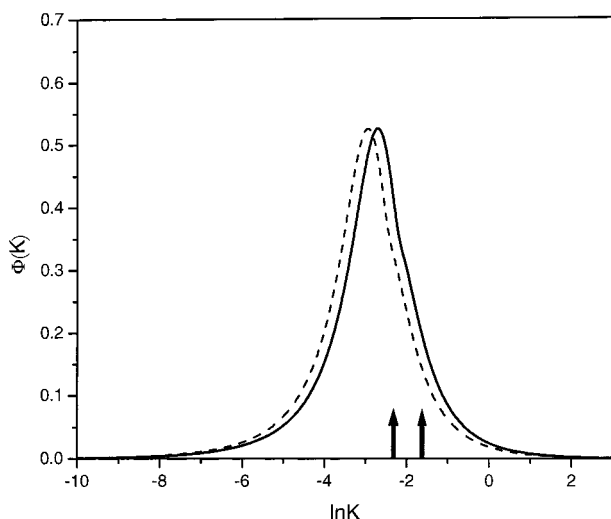


Figure 2. Distribution functions of the equilibrium constants calculated for (R)-PP (continuous line) and (S)-PP (dashed line) on cellulose tribenzoate CSP. The vertical spikes indicate the equilibrium constants obtained by the BL model ($K_{1,1} = K_{2,1}$ and $K_{2,2}$, respectively).

A particular case is interesting and relevant to this work, however. It was shown that, when the local isotherm is Langmuir and the overall adsorption isotherm is Tóth, the equilibrium constant (K) density probability function is given by⁵⁵

$$\Phi(k) = \pi^{-1} \Gamma(k)^{1/\nu} \sin(\nu)^{-1} \arcsin(\sin(\pi\nu)z\Gamma(k)) \quad (32)$$

where

$$\Gamma(k) = \frac{1}{\sqrt{(z^2 + 2 \cos(\pi\nu)z + 1)}} \quad (33)$$

and

$$z = (k/K)^\nu \quad (34)$$

Since our experimental data fit reasonably well the Langmuir model and excellently the Tóth model, it is not unreasonable to assume a local isotherm given by the Langmuir model. The probability density functions for (S)-PP and (R)-PP components calculated with eq 32 are shown in Figure 2 (where for reference we also indicated the equilibrium constant values obtained when the BL model is assumed). The shape of the distribution functions of the two enantiomers is the same. This is explained by the fact that the heterogeneity factor, which controls the shape of the distribution (see eq 32), is the same for both enantiomers. The distributions have different maximums and their shape is not symmetrical. They present an obvious tail toward the low values of the equilibrium constant, indicating that weaker sites contribute significantly to the adsorption at low concentrations.

The energy function distributions derived in this work suggest a complex chiral recognition mechanism, in which weak interactions seem to play a fundamental role. We may assume the same

kind of retention mechanism for both enantiomers since their energy distribution functions have the same shape. However, the different average values for these distributions indicates a different free energy of the reversible diastereomeric association between CSP and enantiomers. This, in turn, could suggest a different matching (entropic effect) between the molecules adsorbed and the stationary phase. Probably the different equilibrium position of the PP aromatic ring with respect to the aromatic rings of the CSP substituents is the main reason for this different equilibrium constant. However, only a systematic study of the effect of temperature on the isotherm shape could permit the separation of the entropic and enthalpic contributions to the adsorption process.

3. Validation of the Isotherm Model: Simulation of Profiles Recorded in Overloaded Conditions. In chromatography, the validation of an isotherm model requires the calculation of overloaded band profiles under well-specified experimental conditions and the comparison of the results with experimental profiles recorded under these conditions. The choice of the best isotherm model to fit the experimental data must be made on this basis. It is not unusual that two different isotherm models that are able to account as well for experimental adsorption data predict significantly different band profiles.

Successful calculations of band profiles using the GR and the POR models require advanced knowledge of several important parameters. These parameters and their values selected according to the particular experimental conditions used are listed in Table 2, as well as the equations used to calculate them. Figure 3a compares the experimental results (symbols) and the calculated profiles (solid line) for a racemic mixture, with a concentration equal to 0.6 g/L and an injection volume of 2 mL. For this calculation, the bulk diffusion coefficient (D_m), calculated according to eq 20, was 0.0017 cm²/min. The external mass-transfer resistance (k_{ext}) was derived using eqs 16 and 19, and the effective diffusion coefficient (D_{eff}) was derived using eq 14. The agreement between the experimental and theoretical results is extremely poor with these values of k_{ext} and D_{eff} . This confirms that the use of the bulk diffusivity, D_m (eq 20) leads to an overestimated value of the effective diffusion coefficient. This result was previously observed and reported by different groups.^{56–61} It was confirmed recently in the case of bovine serum albumin in anion-exchange chromatography.³¹ For this reason, the bulk diffusion coefficients were numerically estimated during the calculation of overloaded profiles under different experimental conditions and used to calculate the corresponding effective diffusion coefficients (through eq 14).

As shown in Figure 3b, the agreement between experimental and theoretical profiles is considerably increased when the calculations are made under exactly the same set of conditions as used for Figure 3a, but with a value of D_m of the order of 1×10^{-4} cm²/min (the typical numerical value obtained in calculations of overloaded profiles). The loading factor (L_d) was derived

(56) Tsou, H. S.; Graham, E. E. *AICHE J.* **1985**, *31*, 1959–1966.

(57) Graham, E. E.; Fook, C. F. *AICHE J.* **1982**, *28*, 245–250.

(58) Skidmore, G. L.; Horstmann, B. J.; Chase, H. A. *J. Chromatogr., A* **1990**, *498*, 113–128.

(59) Fernandez, M. A.; Carta, G. *J. Chromatogr., A* **1996**, *746*, 169–183.

(60) Fernandez, M. A.; Laughinghouse, W. S.; Carta, G. *J. Chromatogr., A* **1996**, *746*, 185–198.

(61) Yoshida, H.; Yoshikawa, M.; Kataoka, T. *AICHE J.* **1994**, *40*, 2034–2044.

(55) Tóth, J.; Rudziński, W.; Waksmundzki, A.; Jaroniec, M.; Sokolowski, S. *Acta Chim. Hung.* **1974**, *82*, 11–20.

Table 2. GR and POR Model Parameters, Their Values under Our Experimental Conditions, and Equations (or Equation Reference Numbers in the Paper) Used To Calculate Them

parameter	value	eq no.
external mass-transfer coefficient, k_{ext} (cm/min)	3.8	16, 19, 20
molecular diffusion coefficient, D_m (cm ² /min)	0.0017	20
dispersion coefficient, D_L (cm ² /min)	0.0032	21
effective diffusion coefficient, D_{eff} (cm ² /min)	2.58×10^{-4}	14, 20
total porosity, ϵ_t	0.715	V_0/V_{col}
external porosity, ϵ_e	0.35	typical value
internal porosity, ϵ_p	0.561	$(\epsilon_t - \epsilon_e)/(1 - \epsilon_e)$

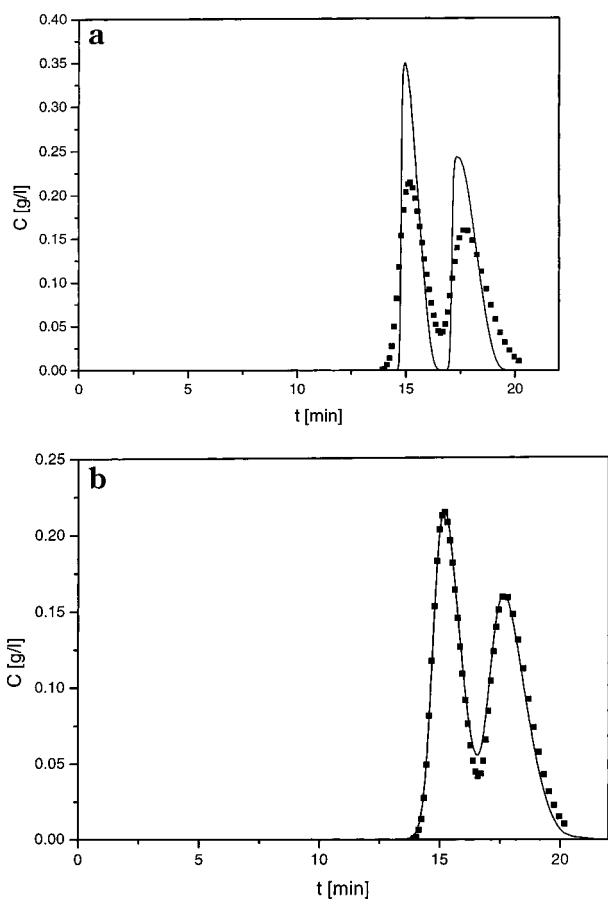


Figure 3. Comparison between experimental (symbols) and calculated (solid lines) band profiles. Racemic mixture concentration, 0.6 g/L; injection volume, 2 mL; $L_f = 0.37\%$. Molecular diffusivities for both components: (a) $D_m = 0.0017$ cm²/min; (b) $D_m = 1.0 \times 10^{-4}$ cm²/min.

from the classical equation²³

$$L_f = \frac{n}{(1 - \epsilon_T)SLq_s} \quad (35)$$

where n is the sample size, ϵ_T is the total column porosity, S is the column cross-sectional area, L is the column length, and q_s is the saturation capacity of the stationary phase (per unit volume). From the isotherm coefficients, the loading factor was 0.37%. The agreement between experimental data and calculated profile is good although the rear part of the experimental peak of the second enantiomer is slightly larger than the calculated one. This may be explained by the presence of some residual impurity in the racemic mixture used, despite its purification.⁴¹

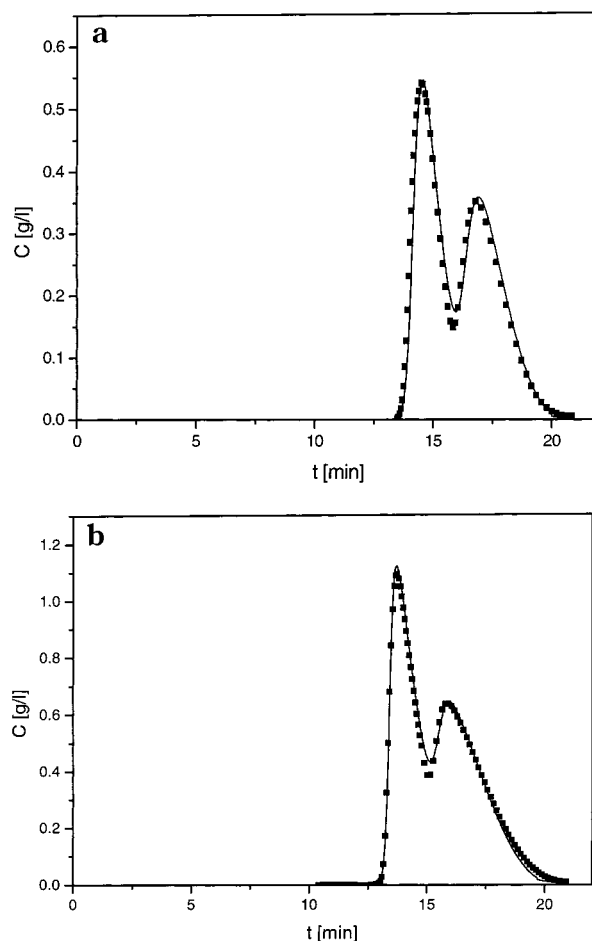


Figure 4. Comparison between experimental (symbols) and calculated (solid lines) band profiles. (a) Racemic mixture concentration, 1.5 g/L; injection volume, 2 mL; $L_f = 0.89\%$; D_{eff} , for the first and the second components, 0.90×10^{-4} and 1.0×10^{-4} cm²/min, respectively. (b) Racemic mixture concentration, 3.0 g/L; injection volume, 2 mL; $L_f = 1.87\%$; same values of D_{eff} as in (a).

The separation of the two enantiomers degrades with increasing amount of feed injected into the column. This is illustrated in Figures 3b–5a corresponding to values of the loading factor increasing from 0.37% (Figure 3b) up to 3.75% (Figure 5a). The height of the valley between the peaks increases with increasing amount injected into the column. Panels a and b of Figure 5 compare the chromatograms obtained with the same amount of feed but different injection profiles. In Figure 5a, the injection time was 1 min (2 mL), in Figure 5b, it was 2 min (4 mL). The model shows a very good ability in fitting the experimental profiles in both cases.

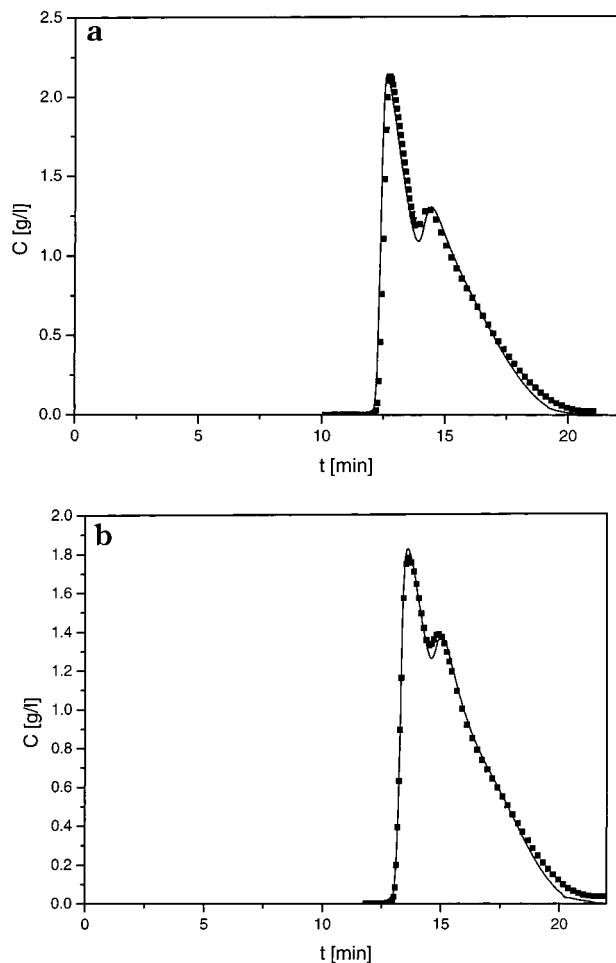


Figure 5. Comparison between experimental (symbols) and calculated (solid lines) band profiles. (a) Racemic mixture concentration, 6.0 g/L; injection volume, 2 mL; $L_f = 3.75\%$; D_{eff} , for the first and second components, 0.77×10^{-4} and 1.3×10^{-4} cm^2/min , respectively. (b) Racemic mixture concentration, 3.0 g/L; injection volume, 4 mL; $L_f = 3.75\%$; D_{eff} , for the first and second components, 0.77×10^{-4} and 1.5×10^{-4} cm^2/min , respectively.

All the calculations illustrated in Figures 3a–5b were performed using both the GR and the POR models. The results of these calculations are practically identical, to the point that the differences between them are too small to be shown. This again confirms the interchangeability between the results of the GR and the POR models when $St/Bi > 5$. Assuming a molecular diffusivity of 1×10^{-4} cm^2/min , this ratio is ~ 100 . However, although predicted, this result had never been illustrated before for a binary mixture. Finally, we should point out that the excellent agreement between experimental and calculated profiles in Figures 3b–5b was obtained only because the diffusion coefficients inside the pores were assumed to be different for the two enantiomers (compare, the values of D_{eff} for (S)-PP and (R)-PP in Table 3). Furthermore, the effective diffusion coefficients (obtained by model identification) depend on the concentration in a nonpredictable way. This means that, most likely, the mass-transfer kinetics implemented in the GR model used in this work is too simple to account properly for the properties of the system studied.

4. External and Internal Mass-Transfer Resistance. The relative intensity of the external and the internal mass-transfer resistances deserves some consideration. The value of k_{ext} is equal

Table 3. Values of the Effective Diffusion Coefficient (D_{eff}) Estimated from the Overloaded Band Profiles Recorded under Different Experimental Conditions (C_{tot} , Racemate Concentration; V_{inj} , Volume Injected; L_f , Column Loading Factor, Eq 35)

$D_{\text{eff}} (\times 10^4 \text{ cm}^2/\text{min})$		experimental conditions			figure no.
(S)-PP	(R)-PP	C_{tot} (g/L)	V_{inj} (mL)	L_f (%)	
1.0	1.0	0.6	2	0.37	3b
0.90	1.0	1.5	2	0.89	4a
0.90	1.0	3	2	1.87	4b
0.77	1.3	6	2	3.75	5a
0.77	1.5	3	4	3.75	5b

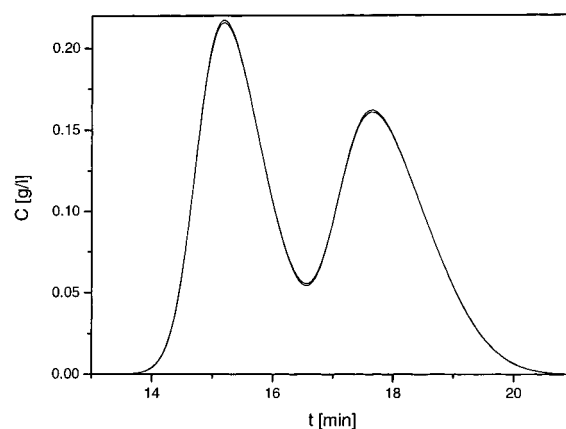


Figure 6. Comparison between band profiles calculated for the racemic mixture with (a) $k_{\text{ext}} = 3.8$ cm/min and $D_L = 0.0032$ cm^2/min and with (b) $k_{\text{ext}} = 1000$ cm/min and $D_L = 0$ (i.e., neglecting the external mass-transfer resistance). Experimental conditions: racemic mixture concentration, 0.6 g/L; injection volume, 2 mL.

to 3.8 cm/min (see Table 2). This was obtained by assuming a diffusivity, $D_m = 0.0017$ cm^2/min , and using eqs 16, 19, and 20. This value is a bulk property of the mobile phase. It cannot be applied to the stagnant solution inside the pores and used to estimate the internal mass-transfer resistance, as shown earlier. Assuming $D_m = 0.0001$ cm^2/min for the diffusivity, eqs 13 and 14 afford an estimate of the internal mass-transfer resistance that leads to $k_{\text{int}} = 0.076$ cm/min . Accordingly, the ratio $k_{\text{ext}}/k_{\text{int}}$ is ~ 50 . This means that the external mass-transfer resistance can be neglected compared with the internal one, at least under the conditions investigated in this work. Figure 6 confirms this point. It shows the peak profiles when (a) the values assumed for the external mass-transfer coefficient, $k_{\text{ext}} = 3.8$ cm/min , and the axial dispersion coefficient, $D_L = 0.0032$ cm^2/min , are finite, and (b) the calculation neglects both the external mass-transfer resistance (a very high k_{ext} value was used in the simulation) and $D_L (= 0$; see figure caption for more details). The profiles corresponding to these two different conditions are practically undistinguishable.

CONCLUSIONS

The model of adsorption used in this work is different from the traditional approach using the BL isotherm model, based on the assumption that the adsorbent surface contains two types of sites, each with a precisely defined Langmuir equilibrium constant. This approach works well for most CSP for which the enantioselective sites are isolated and well identified.^{11,23,47,48} In some

cases, it was successful for cellulose-based CSPs but not in others.^{10,41,47} The isotherm data acquired in this work fitted well to the Tóth isotherm model, suggesting that the CSP used is equally heterogeneous toward both enantiomers. For this isotherm, the adsorption energy probability density function can be expressed in a closed form. This allowed an easy calculation of the distribution.

That the heterogeneity of the surface toward adsorption of either enantiomer is nearly the same can be explained by the nearly identical physicochemical properties of the two enantiomers. This suggests, however, that most of the heterogeneity appears in the nonselective interactions and little in the enantioselective interactions. The distribution energy suggests also that weaker adsorption sites play an important role at high concentrations. In the same time, the separation between the bands decreases, confirming the probable nonselective character of the interactions involving the weaker sites. More detailed conclusions regarding the retention mechanism would require a systematic study of the effect of the temperature on the adsorption isotherm.

The LF and the Tóth isotherm models show the same ability to account for the experimental data at high concentrations. The choice of the Tóth isotherm is justified by considering the different behavior exhibited by the two models at infinite dilution. The LF is inconsistent with the experimental results at low sample sizes: the retention times of the peaks of the two enantiomers do not tend toward infinite with decreasing sample size; the relative retention remains constant at low sample sizes, in contrast with what the LF isotherm model predicts. This precludes its use, in favor of that of the Tóth isotherm model.

The use of the Tóth isotherm model, at least as an empirical model, is suggested for the fitting of equilibrium data acquired for pairs of enantiomers on cellulose-based CSPs. This seems to be a valid alternative to the BL isotherm model, at least for these CSPs. The use of a biTóth model is conceivable, but it would be justified only if data were acquired in an extremely wide concentration range.

Finally, no particular problems arose in connection with the use of the Tóth isotherm model in the calculation of band profiles using the POR and the GR models. The profiles given by the two models were identical, as predicted in this case where the ratio St/Bi is larger than 5.³² The retention times and the peak shapes were, in general, accurately predicted. The external mass-transfer resistance and the mobile-phase dispersion were shown to have a negligible effect on these profiles. However, different values of the pore diffusion coefficient under different experimental conditions had to be assumed to have consistency between simulated and theoretical profiles.

GLOSSARY

a_p	adsorbent particle external surface area
Bi	Biot number
C	concentration in mobile phase
C_p	concentration in the stagnant fluid phase contained inside pores
d_p	equivalent particle diameter
D_L	dispersion coefficient
D_m	molecular diffusion coefficient

D_{eff}	effective (or inside-pore) diffusion coefficient
E_a	adsorption enthalpy
F	equilibrium constant distribution probability density function
k	overall mass transfer coefficient
k_{ext}	external mass transfer coefficient
k_{int}	internal mass transfer coefficient
K	equilibrium constant
K_0	preexponential factor
L	column length
M_s	molecular weight of the solvent
P	equilibrium partial pressure
p	parameter in the Gunn equation
Pe	Peclet number
q	concentration in the solid phase
q_s	saturation capacity
r	radial coordinate
R	dimensionless radial coordinate
R_p	equivalent particle radius
R	gas constant per mole
Re	Reynolds number
Sc	Schmidt number
Sh	Sherwood number
St	Stanton number
t	time
t_p	injection time
T	absolute temperature
u	linear velocity
V_m	molar volume of the liquid solute at its normal boiling point
z	axial coordinate
z	parameter in Tóth energy distribution function

Greek letters

α_A	solute–solvent interaction constant
γ	tortuosity parameter
ΔG	adsorption free Gibbs energy change
ϵ_e	external porosity
ϵ_p	internal (pore) porosity
ϵ_t	total porosity
η	viscosity of fluid phase
θ	local isotherm express as gas pressure function
λ	wavelength
ν	heterogeneity parameter
ρ	fluid density
σ_v^2	dimensionless variance of the distribution of the ratio between fluid linear velocities and average velocity over the column cross section
τ	bed package tortuosity factor
X	local isotherm express as mobile-phase concentration function

Φ	equilibrium constant distribution probability density function
Φ_E	physical domain of the adsorption energies
Φ_K	range of the equilibrium constants

Subscripts

i, j	component index or site index
f	inlet value

Superscripts

0	initial value
—	average value

ACKNOWLEDGMENT

This work was supported in part by Grant CHE-00-70548 of the National Science Foundation and by the cooperative agreement between the University of Tennessee and the Oak Ridge National Laboratory. The authors are grateful to Chiral Technologies (Exton, PA) for the generous gift of Chiralcel OB stationary phase. They thank Djamel E. Cherrack for fruitful advice and discussions.

Received for review July 18, 2001. Accepted September 17, 2001.

AC010751Z